

Sub-picosecond 1030 nm laser-induced damage threshold evaluation of pulsed-laser deposited sesquioxide thin films

Marek Stehlik^a, Goby Govindassamy^b, Janis Zideluns,^a
Fabien Lemarchand,^a Frank Wagner^a, Julien Lumeau^a,
Jacob Mackenzie^b and Laurent Gallais^{a,*}

^aAix Marseille Univ., CNRS, Centrale Marseille, Institut Fresnel, Marseille, France

^bUniversity of Southampton, Zepler Institute, Optoelectronics Research Centre, Highfield, Southampton, United Kingdom

Abstract. Dielectric sesquioxide films (Sc_2O_3 , Y_2O_3 , and Lu_2O_3) were fabricated by pulsed-laser deposition and tested in terms of their laser damage properties for pulses of 500 fs duration, at a wavelength of 1030 nm and at a 10 Hz repetition rate. Comparable tests were performed with magnetron-sputtered thin films of established optical-coating materials (SiO_2 , HfO_2 , and Nb_2O_5), whose results served as a benchmark. The laser-induced damage thresholds of the sesquioxides are comparable to each other, and in the multi-pulse test regime show values close to ones of HfO_2 coatings. A lower damage threshold was observed for the polycrystalline Lu_2O_3 film grown on sapphire compared to single-crystal Lu_2O_3 grown on yttrium aluminium garnet ($\text{Y}_3\text{Al}_5\text{O}_{12}$), attributed to the highly textured morphology and potential for a greater density of defect states in these films. We conclude that pulsed-laser deposition is a potential fabrication method of sesquioxides for use in high-power resistant optical components for ultrashort-pulse lasers. © The Authors. Published by SPIE under a Creative Commons Attribution 4.0 International License. Distribution or reproduction of this work in whole or in part requires full attribution of the original publication, including its DOI. [DOI: 10.1117/1.OE.61.7.071603]

Keywords: laser damage; pulsed-laser deposition; thin films.

Paper 20211495SS received Dec. 18, 2021; accepted for publication Mar. 1, 2022; published online Apr. 23, 2022; corrected May 6, 2022.

1 Introduction

The laser-induced damage threshold (LIDT) of optical components represents the limiting factor of the useful performance of ultrafast solid-state lasers.^{1,2} To improve the LIDT of optical materials, especially optical coatings, considerable efforts have been made to test diverse materials,^{3–5} develop new optimized coating designs,^{6–8} and advanced fabrication methods.^{9–11} Among the plethora of thin-film growth techniques, pulsed-laser deposition (PLD) is considered to be one of the most versatile and powerful.¹² In comparison to other deposition techniques such as sputtering or chemical vapor deposition, PLD enables crystalline thin-film growth at relatively low substrate temperatures.^{13,14} PLD also provides the ability to deposit several multicomponent materials *in situ* with preserved stoichiometry.¹⁵ Since the pioneering PLD work from Smith and Turner in 1965,¹⁶ the technique has been used for deposition of a wide range of materials¹⁷ and recently proved to be a reliable method for optical-coating fabrication.^{18–22}

In the past decade, mirrors based on the combination of HfO_2 , a high-refractive-index material, and SiO_2 , a low-refractive-index material, received considerable attention.^{6,23,24} However, the published sub-picosecond (ps) LIDT results for Sc_2O_3 or Y_2O_3 films, indicate that sesquioxides might be good alternatives for HfO_2 .^{11,25–27} Especially Sc_2O_3 , which is a promising high-refractive-index material that exhibits slightly larger optical bandgap (5.7 eV)²⁸ than HfO_2 (5.55 eV).^{29,30} In fact, electron-beam-deposited Sc_2O_3 and Y_2O_3 thin films, tested at 500 fs and 1030 nm by a single shot and 100 shots at 10 Hz repetition rate, showed LIDTs comparable to that of HfO_2 .¹¹ The laser damage resistance at 500 fs and 1030 nm was also measured for

*Address all correspondence to Laurent Gallais, laurent.gallais@fresnel.fr

ion-beam sputtered Sc_2O_3 for which its 1-on-1 internal damage threshold reached a value of 3.1 J/cm^2 .²⁵ It has to be pointed out that most of the laser damage studies of Sc_2O_3 have been motivated by the development of optical interference coatings in the UV range.^{28,31–33} To the best of our knowledge, all the LIDT studies conducted on sesquioxide films focused either on amorphous or polycrystalline films. Consequently, the results might differ from films produced via PLD, which has the potential to grow single-crystal films.^{21,34,35}

In this work, we prepared pulsed-laser deposited Sc_2O_3 , Lu_2O_3 , and Y_2O_3 sesquioxides and tested them in terms of sub-ps-pulse laser damage. Comparable tests were also performed with magnetron-sputtered (MS) thin films of established optical-coating materials (SiO_2 , HfO_2 , and Nb_2O_5), whose results served as a benchmark. The LIDT values for these more standard materials have been reported in studies comparing them with numerous optical-coating materials.^{3,30}

The thin films studied in this report are intended to be used in dielectric multilayer mirrors or diffractive gratings, particularly grating waveguide structures (GWSs).³⁶ The latter elements offer the possibility to control the temporal,³⁷ spectral,³⁸ or spatial profile of light within or from high-power laser systems.³⁹ This study intends to explore the sesquioxides as potentially interesting materials for use in high-power ultrashort-pulse laser systems. Moreover, the uniqueness of this study lies in the testing of non-traditional sesquioxide materials in their crystalline form. In the case of Lu_2O_3 thin films, we are not aware of any laser damage-related publication in the sub-ps regime.

The following sections describe the deposition techniques used: pulsed-laser deposition and magnetron sputtering. Then the tested samples and their parameters are introduced. This is followed by an explanation of the characterization methods used to qualify the thin-film materials. Afterward, the LIDT station and the procedure employed are described. Finally, the laser damage results are given and their dependence on the number of shots, material bandgap, refractive index, and deposition method is discussed.

2 Sample Fabrication

2.1 Pulsed-Laser Deposition

The deposition of the films investigated in this study was performed with the PLD setup depicted schematically in Fig. 1 and described in more details in Refs. 21, 35, and 40. The targets were fabricated by sintering powders of the materials of interest, which ensures a stoichiometric proportion of the elements, and had a final mass of $\sim 85\%$ of the expected mass for the pure crystalline material of the same volume. Target ablation was achieved using a KrF excimer laser operating at 248 nm, with a pulse duration of $\sim 30 \text{ ns}$ and a repetition rate of 100 Hz, yielding growth rates ranging from 10 (Lu_2O_3) to 20 $\mu\text{m/h}$ (Sc_2O_3). The motion of the target was configured to obtain an effective bi-directional ablation, which was proven to significantly reduce the number of scattering points in the as-grown films.⁴⁰ A Metricon (Model 2010) prism coupler equipped with a #200-P-2 prism, and a HeNe laser source operating at 633 nm was used to determine the refractive index and thickness of the films investigated.

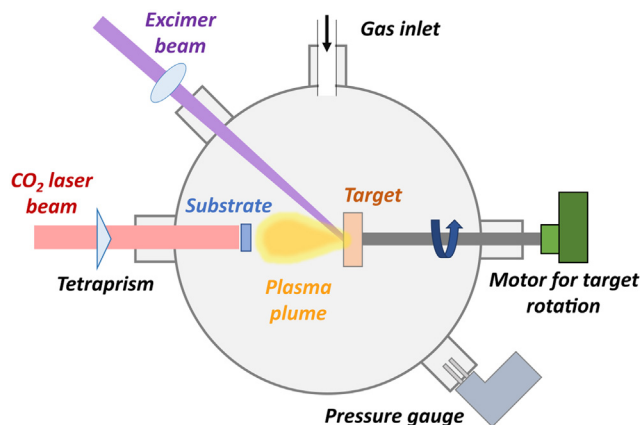


Fig. 1 Pulsed-laser deposition setup.

Table 1 Deposition parameters and lattice properties of the sesquioxide films grown on sapphire (Al_2O_3) or yttrium-aluminum-garnet (YAG) substrates. The measurement of the XRD peaks and lattice constants are detailed in Sec. 3.2. The precision on the position of the (222) XRD peak is limited by the angular resolution of the incident beam, ± 0.01 deg. The film lattice constant is calculated for a Cu $K\alpha$ wavelength of 1.5418 Å and the resolution error is ± 0.004 Å.

Substrate material and orientation	Film	Target ablation fluence (J/cm^2)	Heating power (W)	(222) XRD peak position (deg)	Film lattice constant (Å)
YAG <100 >	Lu_2O_3	1.21	26.7	29.79	10.390
Sapphire <0001 >	Lu_2O_3	1.27	26.2	29.76	10.399
Sapphire <0001 >	Y_2O_3	1.19	18.0	29.10	10.632
Sapphire <0001 >	Sc_2O_3	1.24	24.0	31.50	9.840

To achieve crystalline-film growth, during deposition the rear surface of the substrate was heated by a CO_2 laser operating at $10.6 \mu\text{m}$. The original Gaussian intensity distribution of the beam was transformed by a ZnSe tetraprism⁴¹ into a nearly-uniform $10 \times 10 \text{ mm}^2$ profile, which fits the substrate's dimensions. The substrate temperature used for the deposition of the samples ranged from 950°C to 1100°C , depending on the material.

The background pressure of the vacuum chamber could be tuned by manually adjusting an oxygen gas in-flow. All sesquioxide films analyzed in this report were deposited at a background pressure of $20(\pm 2) \mu\text{bar}$.

The deposition parameters of the investigated samples are listed in Table 1. Optimization of the parameters had been conducted previously and the samples for LIDT measurements were selected based on their crystalline properties and surface homogeneity (in terms of the number of scattering points visible under a dark field microscope).

2.2 Magnetron Sputtering

MS samples were produced with a Helios coater developed by Bühler Leybold optics.⁴² The layers were deposited by the plasma-assisted reactive magnetron sputtering (PARMS) process. Inside the Helios coater, samples are placed on a rotating plate. At first, the sample passes under a mid-frequency dual magnetron, where a thin substoichiometric layer is deposited from a metallic target. Then the sample passes under a radio frequency plasma source where the thin layer is oxidized. The PARMS process, therefore, produces high-density oxide coatings.⁴³ The speed of rotation and power of magnetron is adjusted to deposit $\sim 0.1 \text{ nm}$ of thin-film in each rotation. Each individual thin-film-layer thickness is controlled by *in situ* optical monitoring. Optical measurement is performed at each passing of the substrate under the measurement window. This allows the single-layer thickness to be controlled to better than 1 nm accuracy. Both monochromatic and broadband monitoring can be used in this setup.

Typical pressure inside the vacuum chamber during deposition is 50 nbar. An argon and oxygen mix is used as a process gas for magnetron sputtering, while oxygen is used as the source gas in the plasma for thin-film oxidation. Both high- and low-index materials can be coated within one production cycle.

Previous studies have been conducted on films produced by this machine and their LIDT values compared to a large set of samples produced by different methods and manufacturers, exhibiting LIDT in accordance with the state-of-the-art.^{3,30,44}

3 Characterization of the Thin Films

3.1 Samples to Be Tested

The tested samples were monolayers of Y_2O_3 , Sc_2O_3 , Lu_2O_3 , HfO_2 , Nb_2O_5 , and SiO_2 (See Table 2). The crystalline sesquioxide materials (Y_2O_3 , Sc_2O_3 , and Lu_2O_3) were deposited

Table 2 Tested thin-film materials and their parameters, n means refractive index at 1030 nm wavelength. The Sc_2O_3 , Y_2O_3 , and Lu_2O_3 sesquioxides were PLD-grown in the Optoelectronics Research Centre (Southampton, United Kingdom). The HfO_2 , Nb_2O_5 , and SiO_2 were MS in the Institut Fresnel (Marseille, France).

Material	Thickness (nm)	n	Bandgap (eV)	Deposition	Substrate
Sc_2O_3	1750	1.97	5.74	PLD	Sapphire
Y_2O_3	1310	1.90	5.44	PLD	Sapphire
Lu_2O_3	970	1.91	5.43	PLD	Sapphire
Lu_2O_3	1000	1.91	5.43	PLD	YAG
HfO_2^{a}	250	2.03	5.25	MS	FS
Nb_2O_5	450	2.26	3.41	MS	FS
SiO_2	450	1.47	8 ^b	MS	FS

^a HfO_2 is not pure but contains ~1% to 2% of SiO_2 admixture.⁴⁵

^bThe SiO_2 bandgap was taken from Ref. 44.

on a $\langle 0001 \rangle$ -oriented sapphire substrate. In the case of Lu_2O_3 material, one sample was deposited on a $\langle 100 \rangle$ -oriented yttrium aluminum garnet (YAG) substrate. The amorphous metal oxides (HfO_2 , Nb_2O_5 , and SiO_2) were deposited on fused silica (FS) using the magnetron sputtering process.

3.1.1 Refractive index measurement

The refractive indices of the MS samples were determined by spectrophotometry using numerical fitting methods to the transmittance and reflectance measurements in the low-absorbance spectral region. The values of refractive indices at 1030 nm are listed in Table 2. In the case of pulsed-laser deposited materials, the dispersion curves were determined using ellipsometry. The refractive indices of Y_2O_3 (1.90 @ 1030 nm) and Sc_2O_3 (1.97 @ 1030 nm) correspond well with published values.^{46,47} Extinction coefficients were measured by ellipsometry, however, given the uncertainty of the method, we can only assess that the extinction coefficient values are below 10^{-2} at 1030 nm.

3.1.2 Bandgap measurement

The optical bandgap values of the tested samples were derived from each film's intrinsic absorption coefficient, α , by plotting $(\alpha E)^{1/2}$ as a function of the photon energy E and extrapolating the linear curve to the abscissa axis. The bandgap error margins were estimated using the photon energies corresponding to absorption coefficients of 10^3 and 10^4 cm^{-1} .^{48,49} The value of SiO_2 bandgap was taken from Ref. 44 because the absorption edge could not be reached with our instruments.

3.2 X-Ray Diffraction

Epitaxial growth of the Y_2O_3 , Lu_2O_3 , and Sc_2O_3 films on the $\langle 0001 \rangle$ -cut sapphire was expected to be predominantly in the $\langle 111 \rangle$ -direction, since the lattice mismatch in this orientation is the smallest with substrate orientation, i.e., 4.9%, 2.9%, and 2.5%, respectively. Similarly, $\text{Lu}_2\text{O}_3 \langle 111 \rangle$ has a quasi-perfect lattice match with $\langle 100 \rangle$ -cut YAG, that facilitates the growth of that orientation.

The out-of-plane x-ray diffraction (XRD) patterns from the samples were recorded by a Rigaku Smartlab, equipped with a Ge(220) 2-bounce monochromator. Two different sets of parameters were selected for the scans. A wide scan with a 2θ value from 20 deg to 80 deg and a step size of 0.02 deg was used to compare the proportion of the different orientations

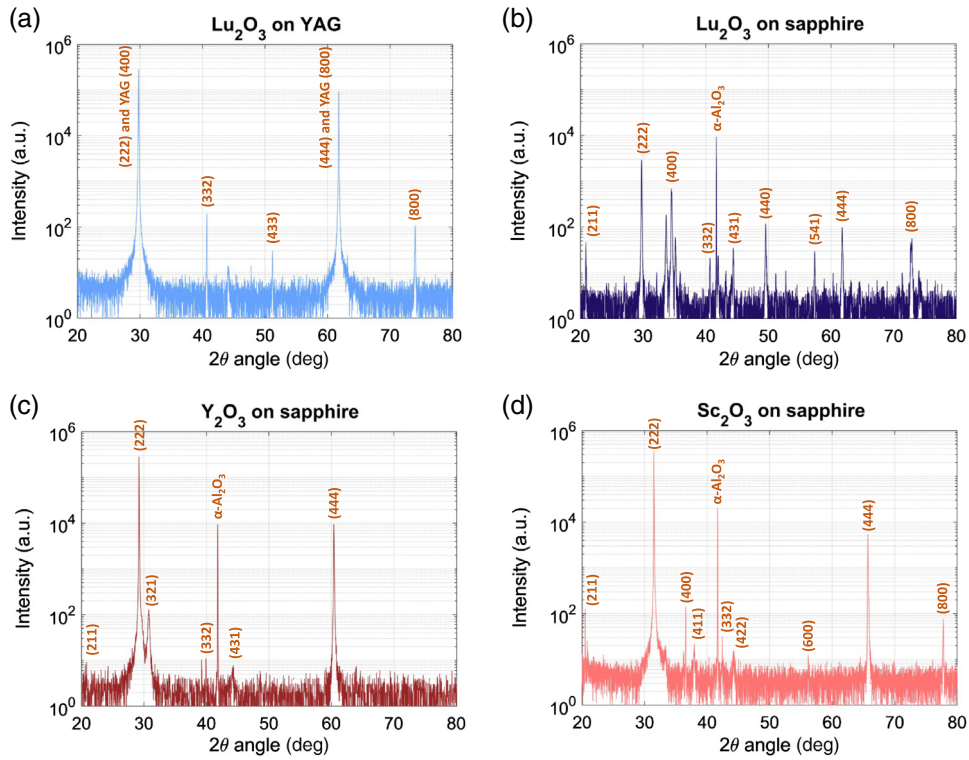


Fig. 2 Wide XRD scans of the PLD samples: (a) Lu_2O_3 film on YAG substrate, (b) Lu_2O_3 film on sapphire substrate, (c) Y_2O_3 film on sapphire substrate, and (d) Sc_2O_3 film on sapphire substrate.

in the film. Since the films were expected to grow preferentially in the $\langle 111 \rangle$ -direction, the (222) diffraction peak was our main peak of interest. Secondly, an additional high-resolution scan with a step size 0.002 deg was made around this primary peak.

Figure 2 displays the XRD patterns of the films with each peak labeled with the corresponding orientation. The Y_2O_3 and Sc_2O_3 films grew primarily in the $\langle 111 \rangle$ -orientation, as demonstrated by the dominance of the (222) peak. The height ratio between the (222)-peak and the peaks corresponding to other orientations is greater than 3000. However, the Lu_2O_3 film grown on sapphire exhibits strong polycrystalline characteristics, with several orientations that have a height ratio of < 30 with the (222) peak. On the contrary, the growth of $\langle 111 \rangle$ -oriented Lu_2O_3 is clearly favored on the YAG substrate: the XRD figure shows also that the (222) peak is 1500 times stronger than the next visible orientation (332) and is nearly perfectly superimposed with the YAG (400) peak at a 2θ angle of 29.8 deg. This aspect is highlighted in the high-resolution XRD pattern of that sample in Fig. 3b, with a clear double-peak lying at 29.8 deg.

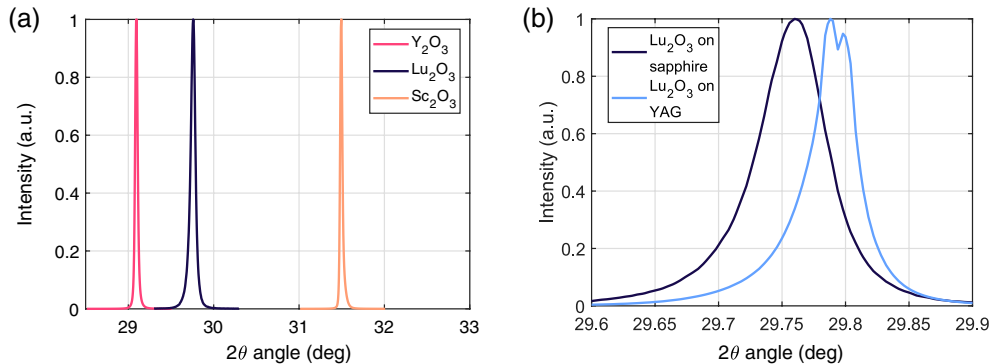


Fig. 3 (222) XRD peaks of the Y_2O_3 , Lu_2O_3 , and Sc_2O_3 films grown on $\langle 0001 \rangle$ -sapphire. (b) (222) XRD peak of the Lu_2O_3 films grown on $\langle 0001 \rangle$ -sapphire and $\langle 100 \rangle$ -YAG.

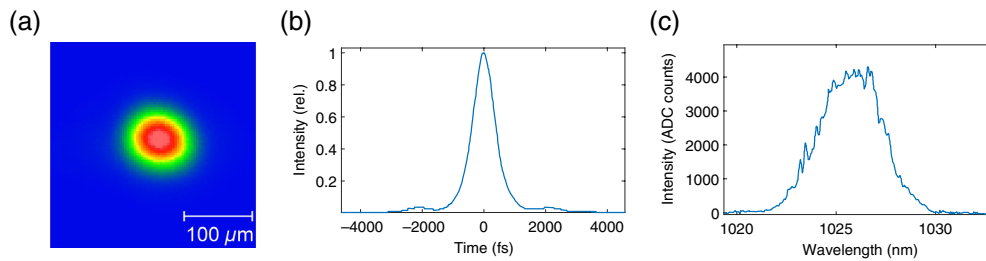


Fig. 4 Laser beam characterization: (a) beam profile in the focal plane, (b) autocorrelation trace, and (c) spectral profile of laser at 1 kHz repetition rate. Effective beam diameter is $84 \mu\text{m}$. Pulse duration full width at half maximum is 525 fs (sech²).

Figure 3 compares the position of the (222) peak of the different films, which was used to calculate their lattice constants. The results, summarized in Table 1, show that the lattice constant of the as-grown films is close to the value reported for the corresponding bulk materials.^{50,51}

4 Description of LIDT Station and Test Procedure

4.1 Test Station

The test station used for LIDT tests is described in Ref. 52 detailing the description of test procedures and metrology methods. For the results reported here in this study, the pulses of nearly Gaussian spatial profile and ~ 500 fs pulse duration at ~ 1030 nm wavelength were incident at a repetition rate of 10 Hz. The maximum achievable pulse energy on a sample was 0.85 mJ. Characterization of the spatial and temporal profiles as well as an energy calibration were carried out before and after the LIDT test campaign. The LIDT tests were performed with samples placed at the focal plane of the lens with 30 cm focal length. The effective beam diameter, as defined by international standards,⁵³ was $84 \mu\text{m}$ in a plane perpendicular to the beam propagation. The LIDT tests were performed in an air environment at a room temperature of 25°C and humidity around 27%. A typical spatial beam profile at the focal plane, autocorrelation trace, and spectral distribution are shown in Fig. 4.

4.2 LIDT Procedure and Damage Detection

Each sample was irradiated at different spots with unique pulse energies that were changed with a $\sim 1\%$ energy increment in order to get statistical data. The procedure was repeated for different numbers of pulses—from single-shot up to 1000 shots at 10 Hz. The LIDT tests were done at a 45-deg incidence angle with P-polarization. The irradiated sites were analyzed *ex situ* using a Zeiss Axiotech differential interference contrast microscope with 20 \times objective magnification. Any observable material modification was evaluated as damage. The damage threshold was determined as the highest fluence that is lower than the lowest fluence causing damage in the experiment. The error bars correspond to the sum of 3σ variations of effective beam area near focal plane ($\sim 3\%$), pulse energy ($\sim 0.7\%$), and a half of pulse energy increment ($\sim 0.5\%$).

4.3 Intrinsic LIDT Fluence

Since the optical layers are the scene of interference effects, the distribution of the electric field inside the layer irradiated by the laser is not homogeneous. The electric field distribution is critical for understanding sub-ps LIDT results since the excitation of dielectrics is governed by electronic processes.² To compare LIDT results, accounting for the conditions influencing the electric field distribution, e.g., angle of incidence, polarization, layer thickness, or refractive index, it is necessary to rescale the LIDT results with the electric field intensity (EFI) maximum (EFI_{max}) within the given layer. Therefore, the fluence values reported in this study correspond to F_{int} intrinsic fluence determined using F_{exp} external fluence and the EFI_{max} and the relation is given by

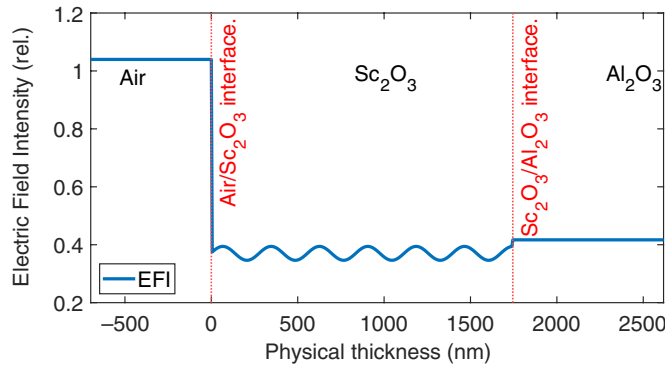


Fig. 5 Distribution of the relative EFI inside a Sc_2O_3 layer of 1745 nm thickness (refractive index 1.97 at 1030 nm wavelength) deposited on a sapphire substrate (refractive index 1.78 at 1030 nm wavelength). Incident beam was P-polarized at an angle of incidence of 45 deg. The EFI is normalized to the incident electric field amplitude in air.

$$F_{\text{int}} = \text{EFI}_{\text{max}} \cdot F_{\text{exp}} = \left| \frac{E_{\text{max}}}{E_{\text{inc}}} \right|^2 \cdot F_{\text{exp}}, \quad (1)$$

where the E_{max} represents the maximum value of the electric field in the layer and the E_{inc} means incident electric field amplitude.⁵⁴ The correction factor of incidence angle during the damage tests (45 deg) is taken into account within the EFI_{max} calculation. The distribution of the relative EFI for the Sc_2O_3 layer used in our experiment is shown in Fig. 5.

5 Laser Damage Results and Discussion

5.1 Deterministic 0 to 1 Transition

To evaluate the uniformity of the tested materials in terms of laser damage, the transition range of the damage probability, as indicated in Fig. 6(a), was calculated for each material and number of

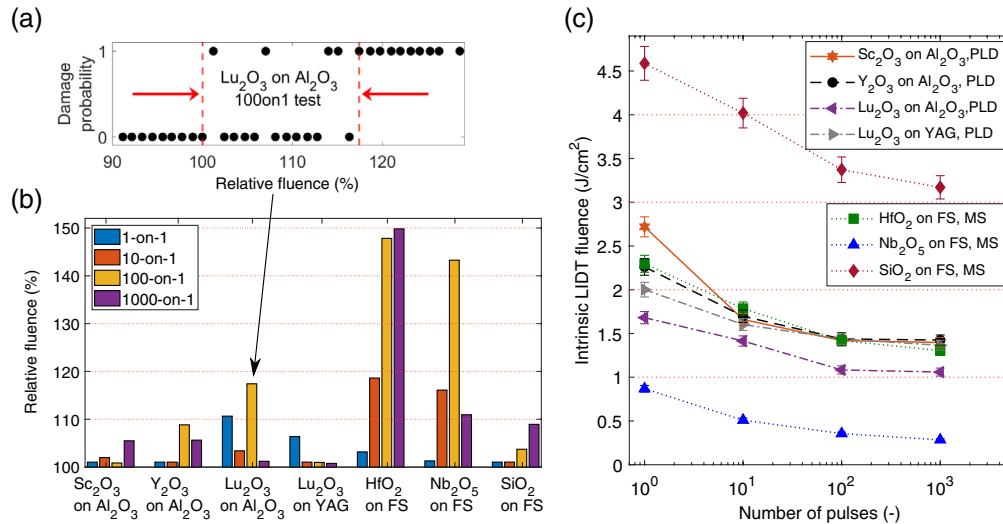


Fig. 6 Laser damage results for materials used in GWS: (a) example of the damage probability results in the case of 100-on-1 tests with Lu_2O_3 deposited on sapphire; (b) transition ranges for the damage probability expressed in relative fluence, as indicated in Fig. 6(a); and (c) intrinsic LIDT fluence as a function of shot number. The Sc_2O_3 , Lu_2O_3 , and Y_2O_3 films were fabricated by pulsed-laser deposition, while HfO_2 , Nb_2O_5 , and SiO_2 by magnetron sputtering. All samples were tested with pulse duration of 500 fs at 1030 nm.

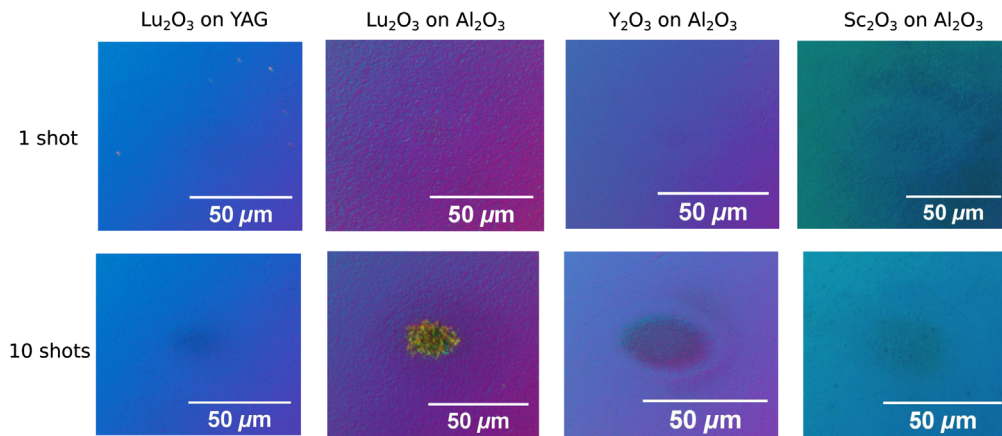


Fig. 7 Laser-induced damage morphologies for the tested crystalline sesquioxide films. Presented spots were irradiated at fluences slightly higher ($\sim 10\%$) than the determined damage thresholds.

shots used, see Fig. 6(b). The 1-on-1 laser damage tests with Sc_2O_3 , Y_2O_3 , SiO_2 , HfO_2 , and Nb_2O_5 show deterministic results, i.e., narrow transition ranges of damage probability from 0 to 1. The transition range of damage probability was only a few percent in fluence, which suggests that the LIDT is limited by intrinsic material properties rather than by defects or impurities caused by the deposition process.⁵⁵ However, in the case of Lu_2O_3 , we found wider transition ranges that could be a consequence of film imperfections, especially in the case of the film grown on sapphire that could be connected to the polycrystalline nature of this film, see Fig. 7. The larger ranges for the multiple-pulse tests may be due to the stochastic formation of deep and shallow traps in the bandgap, which facilitates electron excitation and material modification.²

5.2 LIDT—Single Shot

The intrinsic LIDT fluence as a function of shot number for different thin-film materials is shown in Fig. 6(c). Among the tested materials, the SiO_2 film shows the highest LIDT while Nb_2O_5 shows the lowest. In between, we find the other high-index materials, namely HfO_2 , Sc_2O_3 , Y_2O_3 , and Lu_2O_3 , that are interesting for high-power applications.

HfO_2 , a widely used high-index material in optical mirrors, showed a single-shot LIDT of 2.3 J/cm^2 , which is higher than the values around 2.0 J/cm^2 published in the previous works^{11,56,57} performed under the conditions close to ones used in this study (1030 nm, 500 fs). The higher LIDT of the tested HfO_2 can be explained by the inclusion of SiO_2 in the deposited film, which was estimated from the dispersion curve to be around 1% to 2%.⁴⁵ The effect of the SiO_2 admixture on the HfO_2 damage threshold is in agreement with previous work.³

5.3 LIDT—Multiple Shots

For all materials, the LIDT is decreasing with an increasing number of shots, see Fig. 6(c). The results show a drop of $>20\%$ of the threshold within the first 100 shots. In contrast, at the transition from 100 to 1000 pulses, we observe only a small decrease. These tendencies were already observed in works performed at similar irradiation conditions with metal oxide coatings.^{11,44,58} The gradual decrease is associated with the formation of laser-induced defects, leading to accessible energy levels within the bandgap. The deep or shallow traps can capture electrons from the conduction band even after a sub-threshold irradiation.⁵⁹

In the case of Sc_2O_3 , the drop in LIDT is more noticeable than for the other sesquioxides and reaches that of HfO_2 . The larger 1-on-1 LIDT of Sc_2O_3 compared to HfO_2 was also observed in work with ion-beam sputtered (IBS) films²⁵ which could be related to imperfect damage detection. Going to a higher number of pulses, the HfO_2 deposited on FS, Y_2O_3 on Al_2O_3 , Sc_2O_3 on Al_2O_3 , and Lu_2O_3 on YAG, samples show very similar LIDT, indicating that any of these materials could be recommended for high-power applications, as far as LIDT is concerned.

The 1-on-1 and 100-on-1 LIDT values of Y_2O_3 , Sc_2O_3 , and HfO_2 materials were determined to be close to each other in the study,¹¹ devoted to electron-beam deposited (EBD) single-layers on FS substrates. The LIDT tests were performed at identical conditions to this work (500 fs, 1030 nm, and 10 Hz).

In the case of Lu_2O_3 deposition on an Al_2O_3 substrate, we observe significantly lower LIDT values, which could be explained by the polycrystalline and highly textured nature of the film (Fig. 7). The presence of multiple crystal orientations implies the existence of discontinuities in the lattice that may potentially modify the local bandgap of the material. These boundaries between domains of different orientations may initiate the damage.

5.4 Bandgap

Since the laser-damage initiation in the sub-ps regime is driven by nonlinear ionization, the bandgap represents a critical parameter that correlates with the laser-damage resistance.⁵⁵ The behavior can be explained by taking into account the electron excitation processes playing a dominant role at the beginning of damage formation, i.e., multiphoton and impact ionization.² The intrinsic threshold fluences of tested materials are plotted as a function of their bandgap values in Fig. 8(a). We observe a linear tendency of increasing single-shot LIDT with a larger bandgap value that is in agreement with the studies performed at similar irradiation conditions in Refs. 30 and 60.

The deviations from the linear tendency in Fig. 8(a) can be explained by the challenges faced to observe the material modifications induced by single-shot irradiation, see Fig. 7. Moreover, some of the sesquioxide crystal films exhibit imperfections that include defect sites. For example, the lower LIDT of Lu_2O_3 on sapphire could have been caused by its polycrystalline structure, enabling lower local bandgap values at domain boundaries for different lattice orientations. It should be highlighted that the Tauc method provides a measure of the bandgap at a macroscopic scale, while on the microscopy level there are likely to be numerous defects in the polycrystalline film. Even in the case of the near single-crystal Lu_2O_3 on YAG, the error bars on the bandgap would be larger than that determined from the Tauc measurement method used.

In this work, the LIDT (in J/cm^2) tendency on bandgap E_g (in eV) can be well fitted by the following equation

$$\text{LIDT} = 0.8 \times E_g - 1.93. \quad (2)$$

The equation shows a higher slope, i.e., more dynamic dependence on the bandgap than the empirical description in Ref. 30 derived from results for numerous materials deposited by various methods. The differences from the published data could be explained by the limited number of tested samples or the selected method of bandgap determination.

The bandgap values of sesquioxides are very close to each other with a slightly larger bandgap in the case of Sc_2O_3 , see Fig. 8, whose single-shot LIDT was determined as the highest

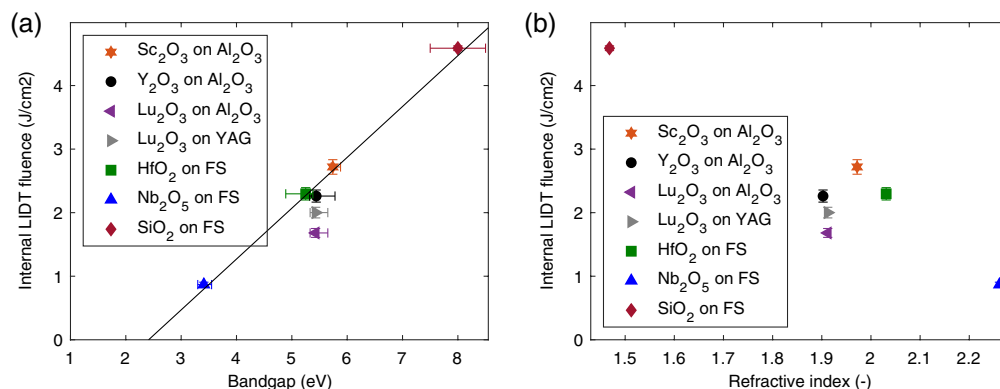


Fig. 8 Single-shot intrinsic LIDT fluence as a function of material bandgap (a) and refractive index (b). The bandgap was determined using the Tauc method.

within the high-index materials. The determined bandgap value for the Sc_2O_3 film tested (5.7 eV) is close to the bandgap of ion-beam sputtered Sc_2O_3 (5.6 eV).²⁵ However, larger bandgaps have been reported for electron-beam deposition (EBD) of Sc_2O_3 (6.5 eV) or Y_2O_3 (6.1 eV)¹¹ compared with the samples tested here grown by PLD, i.e., Sc_2O_3 (5.7 eV) or Y_2O_3 (5.4 eV). It should be noted that care should be taken when comparing bandgaps across publications since the bandgap is not exactly defined and can be determined using different methods.

5.5 Refractive Index

For the design of multilayer components and GWS in our case, the critical parameter is the refractive index. Thus, in Fig. 8(b), we plot the intrinsic 1-on-1 LIDT of the tested materials as a function of refractive index. The results confirm the trend of increasing refractive index with decreasing intrinsic 1-on-1 LIDT, which was also observed in works^{3,30} performed at similar irradiation conditions (500 fs, 1030 nm). Amorphous and single-crystal materials appear to follow the trend, while polycrystalline sesquioxides, such as Lu_2O_3 and Al_2O_3 , seem to be susceptible to a lower LIDT. This could be due to local defects associated with domain boundary interfaces and the highly textured surface. Based on the comparison, Sc_2O_3 seems to be the most promising of the sesquioxides, showing both high damage resistance and a high refractive index value. Furthermore, the pulsed-laser deposited Sc_2O_3 (1.97) shows a higher refractive index @1030nm than the ion-beam sputtered one (1.93)²⁵ or the EBD Sc_2O_3 (1.82).¹¹ The refractive index of the PLD Y_2O_3 samples studied here is the same as that of EBD Y_2O_3 (1.90).¹¹

5.6 Deposition Methods

Thanks to the LIDT studies^{11,25} performed under identical conditions using the same experimental setup like this work (500 fs, 1030 nm), we can compare the LIDT values of sesquioxides deposited by different fabrication methods as shown in Fig. 9. For both Sc_2O_3 and Y_2O_3 , the laser damage resistance of the PLD samples is comparable to that of EBD layers. The thresholds of both PLD and EBD samples indicate a similar fatigue effect—decrease between the 1-on-1 and 100-on-1 thresholds. In the case of 1-on-1 Sc_2O_3 thresholds, the differences between PLD, EBD, and IBS deposition methods can be explained by the difficulty of the detection of material changes. Furthermore, the higher 1-on-1 LIDT of Sc_2O_3 layer fabricated by IBS compared with that of the PLD grown layer could be explained by a 1.6% Si fraction of Sc+Si content in the IBS layer.²⁵

5.7 Sesquioxides in Multilayer Coatings

Lattice-matching constraints strongly limit the potential combinations of materials involving crystalline sesquioxides. Among the materials studied, Sc_2O_3 and $\alpha\text{-Al}_2\text{O}_3$ have the largest

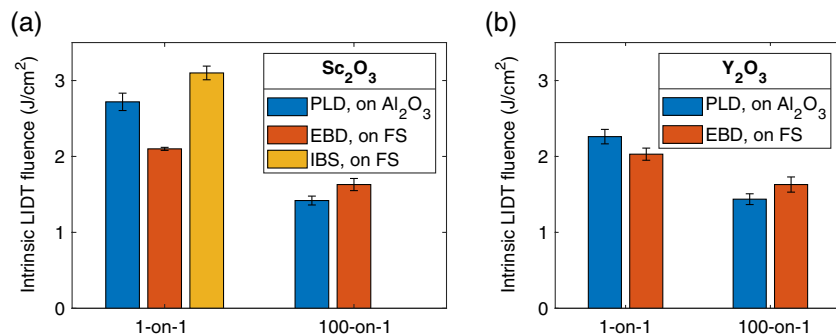


Fig. 9 Intrinsic LIDT fluence for (a) Sc_2O_3 and (b) Y_2O_3 . Comparison of deposition methods. The results of EBD and IBS samples are taken from Refs. 11 and 25, respectively. All samples were tested under identical conditions using the same experimental setup with 500 fs pulse duration at 1030 nm wavelength.

refractive index contrast, i.e., 0.2 at the wavelength of 1030 nm. Despite a lattice mismatch of only 2.5%, the fundamentally different lattice structure of Sc_2O_3 and $\alpha\text{-Al}_2\text{O}_3$ (space group $\text{Ia}\bar{3}$ and $\text{R}\bar{3}\text{c}$, respectively) can potentially make the fabrication of $\text{Sc}_2\text{O}_3/\alpha\text{-Al}_2\text{O}_3$ multilayer coatings more complex than pairs of cubic sesquioxides. However, for example, the lattice mismatch of a $\text{Sc}_2\text{O}_3/\text{Y}_2\text{O}_3$ combination is too large, at 7.6%, for robust thick-multilayer epitaxial growth. Another challenge derives from the lower index contrast between these PLD-grown sesquioxide materials. For instance, a quarter-wave stack of $\text{HfO}_2/\text{SiO}_2$ needs a minimum of 25 layers to reach 99.9% reflectivity at normal incidence for the wavelength of 1030 nm, while an equivalent $\text{Sc}_2\text{O}_3/\alpha\text{-Al}_2\text{O}_3$ mirror would require 73 layers. The resulting multilayer stack would have a full-thickness on the order of 20 μm , which is within the scope of PLD crystalline growth.²² Furthermore, owing to the high deposition rates achievable (15 to 20 $\mu\text{m}/\text{h}$), around 10 times faster than magnetron sputtering, 10's- μm dimensions are entirely feasible within reasonable growth-run times.

6 Conclusion

Sc_2O_3 , Y_2O_3 , and Lu_2O_3 sesquioxide crystalline films, deposited by pulsed-laser deposition, were tested for sub-ps laser damage. Similar intrinsic LIDT fluences of 1.3 to 1.4 J/cm^2 were found for the well-grown sesquioxides, i.e., Sc_2O_3 on sapphire, Y_2O_3 on sapphire, and Lu_2O_3 on YAG, when tested with multiple pulses (100 or 1k).

The LIDT tests on Lu_2O_3 grown on sapphire revealed significantly lower damage thresholds than Lu_2O_3 on YAG. This result is explained by the polycrystalline structure of Lu_2O_3 grown on sapphire, deduced from XRD characterization. The highly textured polycrystalline structure contains discontinuities in the lattice that most probably initiate the damage.

The high-index PLD sesquioxides show high bandgap values indicating good damage resistance in optical coatings. In terms of observed damage thresholds, sesquioxides can compete with HfO_2 , a frequently used high-index material in dielectric multilayers. The study shows that pulsed-laser deposition is a candidate for optical-coating fabrication and that the sesquioxides are promising high-index materials that could be used in applications relating to high-power ultrashort-pulse lasers.

Acknowledgments

This project has received funding from the European Union's Horizon 2020 research and innovation program under the Marie Skłodowska-Curie grant agreement No. 813159. The authors acknowledge the EPSRC for financial support of the Rigaku SmartLab via Grant Nos. EP/K009877/1, EP/K00509X/1, and EP/V035975/1, an EPSRC Doctoral Prize EP/T517859/1, and Grant Nos. EP/N018281/1 and EP/P027644/1. The authors declare no conflicts of interest.

Data, Materials, and Code Availability

Data underlying the results presented in this paper are not publicly available now but may be obtained from the authors upon reasonable request.

References

1. W. Koechner, "Damage of optical elements," in *Solid-State Laser Engineering*, W. T. Thodes et al., Eds., Vol. 1, pp. 680–701, Springer, New York (2006).
2. L. Emmert and W. Rudolph, "Femtosecond laser-induced damage in dielectric materials," in *Laser-Induced Damage in Optical Materials*, D. Ristau, Ed., pp. 127–152, CRC Press, Boca Raton, Florida (2014).
3. B. Mangote et al., "Femtosecond laser damage resistance of oxide and mixture oxide optical coatings," *Opt. Lett.* **37**, 1478 (2012).

4. V. Csajbók et al., “Femtosecond damage resistance of femtosecond multilayer and hybrid mirrors,” *Opt. Lett.* **41**, 3527 (2016).
5. J. Vanda et al., “Comparative LIDT measurements of optical components for high-energy HiLASE lasers,” *High Power Laser Sci. Eng.* **4**, e11 (2016).
6. S. Chen et al., “Femtosecond laser-induced damage of HfO₂/SiO₂ mirror with different stack structure,” *Appl. Opt.* **51**, 6188 (2012).
7. T. Willemsen et al., “Enhancement of the damage resistance of ultra-fast optics by novel design approaches,” *Opt. Express* **25**, 31948 (2017).
8. M. Chorel et al., “Robust optimization of the laser induced damage threshold of dielectric mirrors for high power lasers,” *Opt. Express* **26**, 11764 (2018).
9. J. B. Oliver et al., “Plasma-ion-assisted coatings for 15 femtosecond laser systems,” *Appl. Opt.* **53**, A221 (2014).
10. T. Willemsen et al., “Tunable optical properties of amorphous Tantalum layers in a quantizing structure,” *Opt. Lett.* **42**, 4502 (2017).
11. A. Hervy et al., “Femtosecond laser-induced damage threshold of electron beam deposited dielectrics for 1-m class optics,” *Opt. Eng.* **56**, 011001 (2016).
12. F. Craciun, T. Lippert, and M. Dinescu, “Pulsed laser deposition: fundamentals, applications, and perspectives,” in *Handbook of Laser Micro- and Nano-Engineering*, K. Sugioka, Ed., pp. 1–33, Springer, Cham (2020).
13. D. Rasic et al., “Room temperature growth of epitaxial titanium nitride films by pulsed laser deposition,” *Cryst. Growth Des.* **17**, 6634–6640 (2017).
14. D. Rasic and J. Narayan, “Epitaxial growth of thin films,” Chapter 5 in *Crystal Growth*, V. Glebovsky, Ed., IntechOpen, Rijeka (2019).
15. T. Venkatesan et al., “Laser processing of high-T_c superconducting thin films,” *IEEE J. Quantum Electron.* **25**, 2388–2393 (1989).
16. H. M. Smith and A. F. Turner, “Vacuum deposited thin films using a ruby laser,” *Appl. Opt.* **4**, 147 (1965).
17. K. B. Masood et al., “A comprehensive tutorial on the pulsed laser deposition technique and developments in the fabrication of low dimensional systems and nanostructures,” *Emergent Mater.* **4**, 737–754 (2021).
18. M. Filipescu et al., “Antireflective coatings with high damage threshold prepared by laser ablation,” *Appl. Phys. A* **125**, 815 (2019).
19. A. Bercea et al., “Optical coatings for ELI experiments prepared by laser ablation,” *Rom. J. Phys.* **63**, 606 (2018).
20. E. N. Sirjita et al., “Properties of hafnium and aluminium silicates coatings obtained by PLD,” *Coatings* **11**, 753 (2021).
21. J. J. Prentice et al., “Yb-doped mixed-sesquioxide films grown by pulsed laser deposition,” *J. Cryst. Growth* **491**, 51–56 (2018).
22. K. A. Sloyan et al., “Crystalline garnet Bragg reflectors for high power, high temperature, and integrated applications fabricated by multi-beam pulsed laser deposition,” *Appl. Phys. Lett.* **101**, 081117 (2012).
23. L. O. Jensen et al., “Investigations on SiO₂/HfO₂ mixtures for nanosecond and femtosecond pulses,” *Proc. SPIE* **7842**, 68–77 (2010).
24. L. Lamaignère et al., “Round-robin measurements of the laser-induced damage threshold with sub-picosecond pulses on optical single layers,” *Opt. Eng.* **60**, 031005 (2020).
25. M. Mende et al., “Laser damage resistance of ion-beam sputtered Sc₂O₃/SiO₂ mixture optical coatings,” *Appl. Opt.* **52**, 1368 (2013).
26. C. S. Menoni et al., “Advances in ion beam sputtered Sc₂O₃ for optical interference coatings,” *Proc. SPIE* **7842**, 784202 (2010).
27. E. M. Krous et al., “Scandium oxide thin films deposited by dual ion beam sputtering for high-power laser applications,” in *Opt. Interference Coatings*, FA10, OSA, Tucson, AZ (2010).
28. D. Grosso and P. Sermon, “Scandia optical coatings for application at 351 nm,” *Thin Solid Films* **368**, 116–124 (2000).
29. J. Aarik et al., “Optical characterization of HfO₂ thin films grown by atomic layer deposition,” *Thin Solid Films* **466**, 41–47 (2004).

30. L. Gallais and M. Commandré, "Laser-induced damage thresholds of bulk and coating optical materials at 1030 nm, 500 fs," *Appl. Opt.* **53**, A186 (2014).
31. F. Rainer et al., "Scandium oxide coatings for high-power UV laser applications," *Appl. Opt.* **21**, 3685 (1982).
32. F. Rainer et al., "Materials for optical coatings in the ultraviolet," *Appl. Opt.* **24**, 496 (1985).
33. S. Tamura et al., "Laser-damage threshold of $\text{Sc}_2\text{O}_3/\text{SiO}_2$ high reflector coatings for a laser wavelength of 355 nm," *Thin Solid Films* **228**, 222–224 (1993).
34. S. J. Beecher et al., "Ytterbium-doped-garnet crystal waveguide lasers grown by pulsed laser deposition," *Opt. Mater. Express* **7**, 1628 (2017).
35. G. A. Govindassamy et al., "Effect of laser repetition rate on the growth of Sc_2O_3 via pulsed laser deposition," Submitted to *Appl. Phys. A* (2022).
36. G. Quaranta et al., "Recent advances in resonant waveguide gratings," *Laser Photonics Rev.* **12**, 1800017 (2018).
37. M. Rumpel et al., "Broadband pulse compression gratings with measured 99.7% diffraction efficiency," *Opt. Lett.* **39**, 323 (2014).
38. M. M. Vogel et al., "Single-layer resonant-waveguide grating for polarization and wavelength selection in Yb:YAG thin-disk lasers," *Opt. Express* **20**, 4024 (2012).
39. M. A. Ahmed et al., "Applications of sub-wavelength grating mirrors in high-power lasers," *Adv. Opt. Technol.* **1**, 381–388 (2012).
40. J. J. Prentice et al., "Particulate reduction in PLD-grown crystalline films via bi-directional target irradiation," *Appl. Phys. A* **125**, 152 (2019).
41. T. C. May-Smith et al., "Design and performance of a ZnSe tetra-prism for homogeneous substrate heating using a CO_2 laser for pulsed laser deposition experiments," *Appl. Opt.* **47**, 1767–1780 (2008).
42. D. Depla, S. Mahieu, and J. Greene, "Sputter deposition processes," Chapter 5 in *Handbook of Deposition Technologies for Films and Coatings*, P. M. Martin, Ed., 3rd ed., pp. 253–296, William Andrew Publishing, Boston (2010).
43. M. Scherer, "Magnetron sputter-deposition on atom layer scale," *Vak. Forsch. Prax.* **21**, 24–30 (2009).
44. D.-B. Douti, L. Gallais, and M. Commandré, "Laser-induced damage of optical thin films submitted to 343, 515, and 1030 nm multiple subpicosecond pulses," *Opt. Eng.* **53**, 122509 (2014).
45. H. Hagedorn et al., "Plasma assisted reactive magnetron sputtering of demanding interference filters," in *SVC TechCon*, O–24, Santa Clara, CA (2012).
46. Y. Nigara, "Measurement of the optical constants of yttrium oxide," *Jpn. J. Appl. Phys.* **7**, 404–408 (1968).
47. A. Belosludtsev et al., "Correlation between stoichiometry and properties of scandium oxide films prepared by reactive magnetron sputtering," *Appl. Surf. Sci.* **427**, 312–318 (2018).
48. O. Stenzel et al., "Mixed oxide coatings for optics," *Appl. Opt.* **50**, C69–C74 (2011).
49. E. C. Freeman and W. Paul, "Optical constants of RF sputtered hydrogenated amorphous Si," *Phys. Rev. B* **20**, 716–728 (1979).
50. C. Krankel, "Rare-earth-doped sesquioxides for diode-pumped high-power lasers in the 1-, 2-, and 3- μm spectral range," *IEEE J. Sel. Top. Quantum Electron* **21**, 250–262 (2015).
51. Y. Kuzminykh, A. Kahn, and G. Huber, " Nd^{3+} doped Sc_2O_3 waveguiding film produced by pulsed laser deposition," *Opt. Mater.* **28**, 883–887 (2006).
52. M. Stehlik et al., "Beam-size effects on the measurement of sub-picosecond intrinsic laser induced damage threshold of dielectric oxide coatings," *Appl. Opt.* **60**, 8569–8578 (2021).
53. ISO 21254-1:2011, "Lasers and laser-related equipment—test methods for laser-induced damage threshold—part 1: definitions and general principles," Tech. Rep., International Organization for Standardization, Geneva (2011).
54. K. Ohta and H. Ishida, "Matrix formalism for calculation of electric field intensity of light in stratified multilayered films," *Appl. Opt.* **29**, 1952 (1990).
55. M. Mero et al., "Scaling laws of femtosecond laser pulse induced breakdown in oxide films," *Phys. Rev. B* **71**, 115109 (2005).
56. A. Hervy et al., "Electron-beam deposited materials for high-reflective coatings: femtosecond LIDT," in *Opt. Interference Coat.*, FA.4, OSA, Whistler, Canada (2013).

57. L. Gallais et al., "Laser-induced damage of hafnia coatings as a function of pulse duration in the femtosecond to nanosecond range," *Appl. Opt.* **50**, C178–C187 (2011).
58. D. N. Nguyen et al., "The effect of annealing on the subpicosecond breakdown behavior of hafnia films," *Proc. SPIE*, **7132**, 71320N (2008).
59. L. A. Emmert, M. Mero, and W. Rudolph, "Modeling the effect of native and laser-induced states on the dielectric breakdown of wide band gap optical materials by multiple subpicosecond laser pulses," *J. Appl. Phys.* **108**, 043523 (2010).
60. B. Mangote et al., "A high accuracy femto-/picosecond laser damage test facility dedicated to the study of optical thin films," *Rev. Sci. Instrum.* **83**, 013109 (2012).

Biographies of the authors are not available.